RESEARCH ARTICLE

ADVANCED HEALTHCARE MATERIALS
www.advhealthmat.de

Unraveling the Heterogeneity of Cargo Distribution in the Exogenous Association of Proteins With Extracellular Vesicles

*Karl Normak, Marcell Papp, Carolina Paganini, Andrea Zendrini, Paolo Bergese, Dorothea Pinotsi, and Paolo Arosio**

Extracellular vesicles (EVs) are emerging as promising nanocarriers for delivering molecules, including proteins. Various exogenous methods are proposed for loading EVs with specific cargo proteins. While the loading yield and the heterogeneity of cargo distribution are crucial quality attributes, a comprehensive quantification of these properties is still lacking. Here, we characterize the heterogeneity of EVs loaded with a model cargo protein, GFP, using various exogenous methods. A combination of biophysical methods is applied to quantify the overall yield and cargo distribution at both the ensemble and single-particle levels. Among the loading methods evaluated, electroporation is most effective for associating GFP with EVs. However, the GFP molecules per vesicle is fewer than 100, representing approximately 4% of the maximum protein capacity that EVs can potentially accommodate. Across all loading methods, the distribution of protein content per vesicle displays significant heterogeneity and follows an exponential decay function, with a higher prevalence of vesicles featuring lower protein content and fewer with higher content. Moreover, loading efficiency increases with EV size. This study shows that overall yields of exogenous loading methods to associate proteins with EVs remain modest and the resulting distribution of cargo proteins associated with EVs is highly heterogeneous.

1. Introduction

Extracellular vesicles (EVs) are particles secreted by all cells into the extracellular space,[1–4] acting as messengers that mediate diverse biological processes.[5,6] EVs are capable of delivering genetic information, signalling molecules, proteins, and lipids to recipient cells, thereby facilitating phenotypic changes and triggering functional responses.[5,7] The ability of EVs to transmit chemical signals between specific cells and cross biological membranes has led to efforts in developing them as drug delivery vectors for cargo molecules,[8] including small molecules,[9,10] proteins,[11] and nucleic acids.[12–14] In the case of recombinant proteins, this approach holds promise for improving targeted delivery and opening new avenues for protein intracellular delivery, which is currently limited.[15]

However, associating large biomacromolecules with EVs in a consistent way remains a challenge. Different methods have been proposed for introducing biomolecules into EVs, which can be categorized as either endogenous[16,17] or exogenous[10–12] approaches. Endogenous loading involves genetically engineering cells to encode and sort cargo proteins into EVs. In exogenous loading, cargo molecules are mixed with isolated EVs before applying a physical (e.g., electroporation[11]) or chemical stress (e.g., saponins[9]), which allows the cargo to be associated with EVs through transient pores generated in the EV membrane. Similar approaches have also been applied to generate hybrid materials based on nanoparticles and vesicles.[18] Moreover, combining different physical and chemical stresses can have synergistic effects for cargo association.[19]

Although these methods proved successful, each approach presents limitations. For instance, endogenous loading of proteins can yield highly heterogeneous populations of loaded EVs, and the loading efficiency can vary depending on the specific EV-sorting protein considered.[16,17] Furthermore, the desired cargo may have unwanted effects on the viability and expression level of the EV-producing cell.

Exogenous loading, due to geometrical constraints, has inherent limitations in terms of yield, defined as protein loaded per total amount of protein introduced in the system. Since the volume fraction of EVs is typically around 0.001%, the amount of

K. Normak, M. Papp, C. Paganini, P. Arosio
Department of Chemistry and Applied Biosciences
ETH Zurich
Zurich 8093, Switzerland
E-mail: paolo.arosio@chem.ethz.ch

A. Zendrini, P. Bergese
Department of Molecular and Translational Medicine
University of Brescia
Brescia 25123, Italy

A. Zendrini, P. Bergese
Center for Colloid and Surface Science (CSGI)
Florence 50019, Italy

D. Pinotsi
Scientific Center for Optical and Electron Microscopy
ETH Zurich
Zurich 8093, Switzerland

The ORCID identification number(s) for the author(s) of this article can be found under https://doi.org/10.1002/adhm.202403991

DOI: 10.1002/adhm.202403991

protein associated with EVs remains minuscule compared to the total protein amount, even in case of successful loading. This requires the development of effective fractionation methods to separate EVs from free cargos. Moreover, it remains unclear the number of cargo proteins that can be loaded into individual EVs and their distribution within the EV population. Recent studies focusing on small molecule cargos, such as doxorubicin, have indicated a highly heterogeneous distribution of cargos within the EV population.[19–21]

Heterogeneity is present in nearly all nanotherapeutics, including simpler synthetic nanoparticles.[22–24] This heterogeneity is even more pronounced in biological EVs,[25] and is further amplified by cargo association.[19–21,26] Such heterogeneity of EVs impacts their behavior in vivo and in vitro, complicating analytical characterization, optimization and clinical translation.[2,8,25–28]

Indeed, differences in EV size,[29] surface composition,[30] and cargo content[19–21,31] can dramatically influence their targeting efficiency, pharmacokinetics, and immune clearance.[32] For example, heterogeneous EV populations can lead to inconsistent delivery of therapeutic payloads to target tissues, increased uptake by off-target cells or immune cells, and rapid systemic clearance, ultimately compromising therapeutic efficacy, and reproducibility.[22–24] This heterogeneity has been shown to limit the translational success of EV formulations in preclinical models and complicate their clinical development. This underlines the need for characterization strategies to quantify EV heterogeneity of cargo distribution within EV populations.

In this study, we employ ensemble and single-particle biophysical methods to determine the yield and loading heterogeneity[33] of common exogenous methods used to associate cargo proteins with EVs. Specifically, we compare the efficiency of electroporation,[34] sonication,[11] and freeze-thaw cycles[35] in associating the model cargo GFP with EVs derived from HEK293-F cells[8,36–39] We characterize the loading at the ensemble level using bead-based flow cytometry and a recently developed method based on size exclusion chromatography coupled with fluorescence detection and light scattering.[39] Furthermore, we apply super resolution microscopy (dSTORM) combined with the density-based clustering algorithm DBSCAN to quantify the cargo distribution in individual EVs, achieving a resolution down to the single GFP level.

2. Results and Discussion

2.1. Initial Comparison of Exogenous Loading Methods With Ensemble Level Biophysical Approaches

The efficiency of GFP association with EVs was initially assessed at the ensemble level using two analytical methods.

The first method involved separating EVs from free cargo by size exclusion chromatography (SEC). The resulting eluting populations were then analyzed using a combination of fluorescence (FLD) and multi-angle light scattering (MALS) techniques[39] These techniques enable the measurement of the concentration and size of EVs as well as of specific fluorescently labelled components that either co-elute with EVs or are free in solution.[39] By applying this approach we can therefore evaluate the loading efficiency from the fluorescent signal, and the potential EV loss during the treatment process by measuring the concentration and size of EVs.[39] As second method, we employed bead-based flow cytometry (FC), where we monitored the GFP fluorescence signals of EV captured by anti-CD81 antibody covered beads. We note that in this work we measure cargo proteins strongly associated with EVs, without differentiating between proteins loaded inside EVs and molecules strongly adsorbed on the surface of the EVs, which cannot be dissociated during the chromatographic separation.

According to the SEC-MALS-FLD analysis, electroporation exhibited the highest efficiency in terms of total amount of cargo protein associated with EVs (15 fmol of loaded GFP out of the 400 000 fmol introduced in solution) (**Figure 1A**). This corresponds to a loading efficiency of approximately 0.004%. In contrast, sonication, freeze-thaw and incubation led to a low total loaded GFP amount of less than 2 fmol (loading efficiency of less than 0.0005 %).

In addition to quantifying loading yields by FLD, the MALS analysis reports on the loss of particles or changes in size that can result from the applied loading stress. The number of particles after electroporation was similar to incubation (approximately 93%), while a significantly lower number of particles was recovered after freeze-thaw and sonication (approximately 18% for both methods) (Figure 1B). Furthermore, a similar diameter of 190 nm was measured after electroporation and incubation, while a smaller average particle size was observed after sonication and freeze-thaw (Figure S4, Supporting Information).

The measurement of amount of cargo loaded and of number of recovered EVs enabled us to evaluate the average number of GFP molecules loaded per particle (Figure 1C). Electroporation led to the largest amount of GFPs per vesicle (56 GFP molecules per particle), much larger than the average of 4 GFPs molecules per particle obtained by incubation. Freeze-thawing was the second best method in terms of cargo molecules per EV (19 GFP molecules per particle) but exhibited significant particle loss (Figure 1B). This demonstrates the importance of measuring the amount of cargo per EV.

However, the SEC-MALS-FLD may lead to a false positive signal due to possible presence of GFP aggregates of similar size of EVs, which may be formed upon application of the loading methods.[13] Therefore, it is important to confirm the association of the cargo with the vesicles using alternative methods.

We confirmed these results by applying bead-based flow cytometry using anti-CD81 beads. In good agreement with the results of the SEC-MALS-FLD analysis, electroporation, and freeze-thaw showed a higher average mean GFP fluorescence (Figure 1D), indicating that a higher amount of GFP has been associated with the analyzed EVs. Furthermore, after electroporation and freeze-thaw, beads characterized by high GFP fluorescence were observed (Figure 1D).

Overall, among the methods tested in this study with our EVs, both SEC-MALS-FLD and FC indicated that electroporation is a successful exogenous approach to associate GFP with EVs. We expect that tailored optimization of different methods for specific EV-cargo systems can improve their yield. However, the overall yield of encapsulation remained a challenge for all approaches.

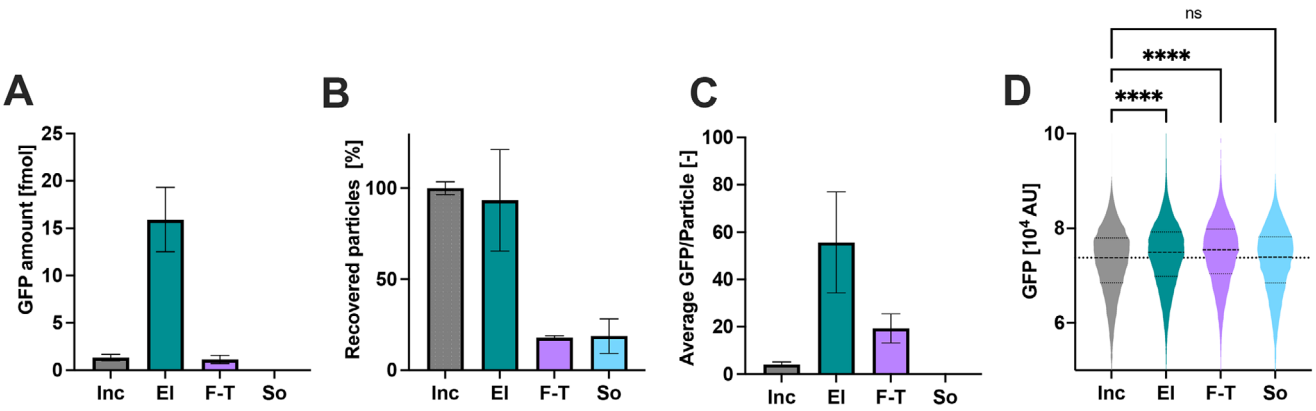

Figure 1. Ensemble characterization of exogenous association of GFP with EVs. A) Total amount of loaded GFP (fmol) characterized by SEC-FLD. The data are represented as mean +/- standard deviation of three replicates (n=3). B) Percentage of recovered particles, with 100% corresponding to average value obtained after incubation. C) Average GFP per particle characterized by SEC-MALS-FLD. D) Violin plots showing the distribution of GFP fluorescence in bead based flow cytometry. The measured GFP fluorescence is on average higher after EI and F-T, which confirms loading of CD81+ EVs.The distribution consists of a minimum 12000 individually quantified beads. Post hoc analysis: Ordinary one way ANOVA **** - P-value <0.0001. Inc – Incubation, EI – Electroporation, F-T – Freeze-Thaw, So – Sonication.

2.2. Multiparametric Characterization of Single EVs by dSTORM-DBSCAN

In addition to the average yield, it is important to characterize the distribution of cargo loading in the EV population, which strongly affects the bioactivity of loaded EVs.

To this aim, we analyzed the loading efficiency at the single-particle level by direct stochastic optical reconstruction microscopy (dSTORM). This single-molecule super-resolution imaging method allows surpassing the diffraction limit of light microscopy (Figure S5A, Supporting Information) and achieve the resolution required to distinguish single vesicles at a length scale of 10–20 nm (Figure S5B, Supporting Information).[40,41] We analyzed the localization data by Density-Based Spatial Clustering of Applications with Noise (DBSCAN) (Figure S5C, Supporting Information).[42,43] In a nutshell, the algorithm clusters high density datapoints, excluding noise, and allows automatic detection of vesicles from the data while avoiding artifacts and bias from image reconstruction. Additional details are reported in Figures S6 and S7 (Supporting Information). Before applying the method for the characterization of cargo association at the single particle level, we validated the different properties characterized with more defined liposome and EV samples.

We first validated the method to determine the size distribution of particles by preparing and analyzing four populations of liposomes characterized by different size distributions in the range from 50 to 400 nm (see Experimental Section). The size distributions measured by dSTORM were in excellent agreement with the results obtained with nanoparticle tracking analysis (NTA) (Figure S8A–C).

Next, we applied dSTORM to co-localize two EV surface markers (CD81 and CD63) using fluorescently labelled antibodies (antiCD81-AF488 and antiCD63-AF647). The representative localization data obtained from dSTORM is shown in **Figure 2**A and a close up of a representative vesicle is shown in Figure 2B. 80% of the total detected vesicles were positive for CD81, 50% were positive for CD63, and 30% were positive for both markers (Figure 2C).

In addition, dSTORM allows to reconstruct the size distribution of sub-populations characterized by different biomarkers. We found that the CD81+ and CD63+ sub-populations have an overlapping size distribution, while the size distribution of the sub-population which is positive to both markers is slightly larger (Figure 2D).

dSTORM combined with DBSCAN can also be applied to characterize the surface marker distribution on the vesicles from the analysis of the localizations of the different signals. After analysing the localizations of the different markers, it emerges that two markers of the same type (i.e., CD63) are almost always closer than 10 nm (Figure 2E). In contrast, the distance between the nearest localizations of markers of different types (i.e., CD81 to CD63) is almost always larger than 10 nm. These results indicate a patchy distribution of the CD81 and CD63 markers on the EV, in agreement with previously published work.[40]

Finally, we described the morphology of the EV population with the Polsby-Popper (PP) compactness test, which measures the compactness of an object with a value ranging from 0 to 1 (corresponding to a circle).[44] The different sub-populations had similar average PP compactness value of approximately 0.8 (Figure S9, Supporting Information).

2.3. Characterization of Exogenous Loading at the Single Vesicle Level by dSTORM

We next aimed at characterizing the exogenous loading by measuring the co-localization of GFP and EVs at the single vesicle level by direct stochastic optical reconstruction microscopy. EVs were stained with anti-CD63 antibody. Free GFP and GFP weakly bound to EVs were removed by size-exclusion chromatography before imaging.

Figure 3 shows representative co-localization results, with GFP (in blue) and CD63 (in red) signals which are only partially co-localized after the loading process. GFP associated with each vesicle was quantified by considering the photophysical properties of GFP (see Experimental Section).[41–43,45,46]

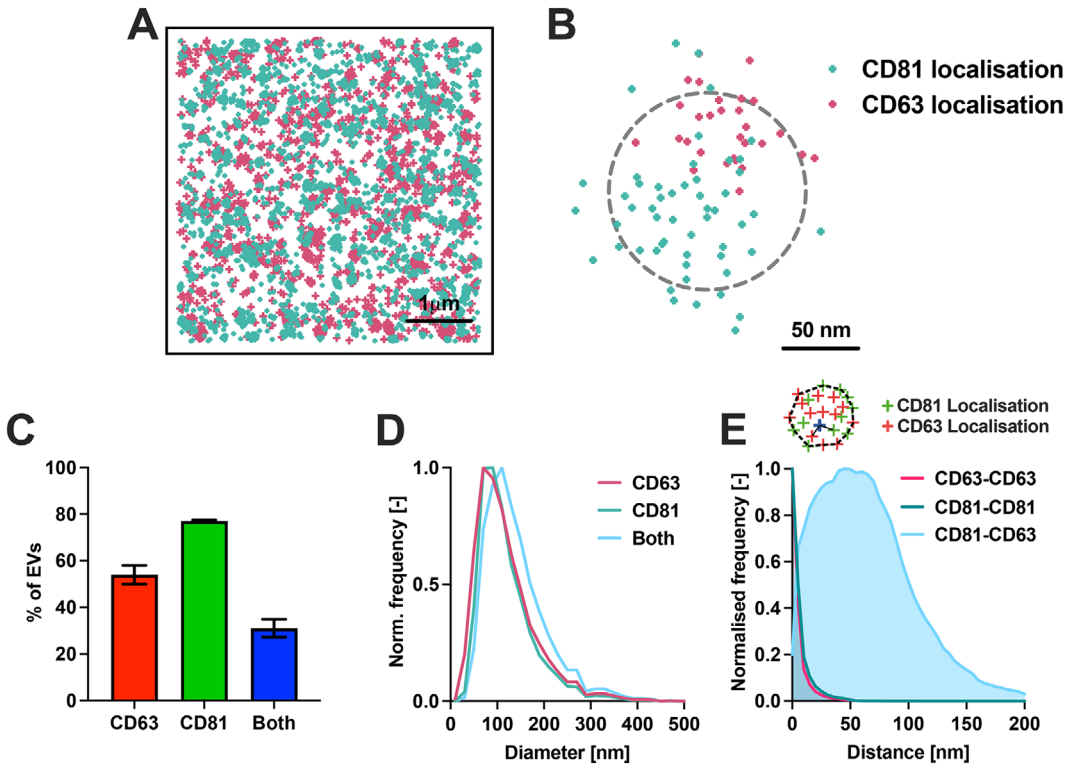

Figure 2. Characterization of EVs by dSTORM. A) Representative localization data after pre-processing. B) Representative localizations of a single EV. Grey circle illustrates the outline of the particle. C) Population of vesicles positive for CD63, CD81 and both markers. The data are represented as mean +/- standard deviation of three replicates (n=3) D) Diameter distribution of the different sub-populations characterized by different markers. The distributions consist of a minimum 2000 individually characterized vesicles. E) Distance distribution between nearest CD63 and CD81 localizations. The distributions consist of a minimum 200000 individually measured distances between localizations.

In agreement with ensemble techniques, dSTORM-DBSCAN analysis showed that electroporation is the most efficient loading method, with 33% of EVs co-localizing with GFP in contrast to the 5% observed after incubation (**Figure** 4A). However, it is interesting to note that the higher sensitivity of the single particle microscopy analysis revealed some level of co-localization also after the sonication treatment, indicating that this method can lead to a small amount of encapsulation which was not detected by either SEC-FLD-MALS or bead-based flow cytometry (Figure 1).

The CD63+ sub-population did not change significantly in size as a result of the loading stresses (Figure 4B). Only after electroporation the mean EV diameter increased from 100 to 115 nm. Moreover, the size distribution of EVs after loading by electroporation shows the presence of vesicles with size of 200–300 nm, which are absent with the other treatments (Figure 4B).

We analyzed possible changes in EV morphology upon application of the loading stresses by measuring their compactness. All tested loading methods have only a minor, although statistically significant, effect on the mean compactness of the

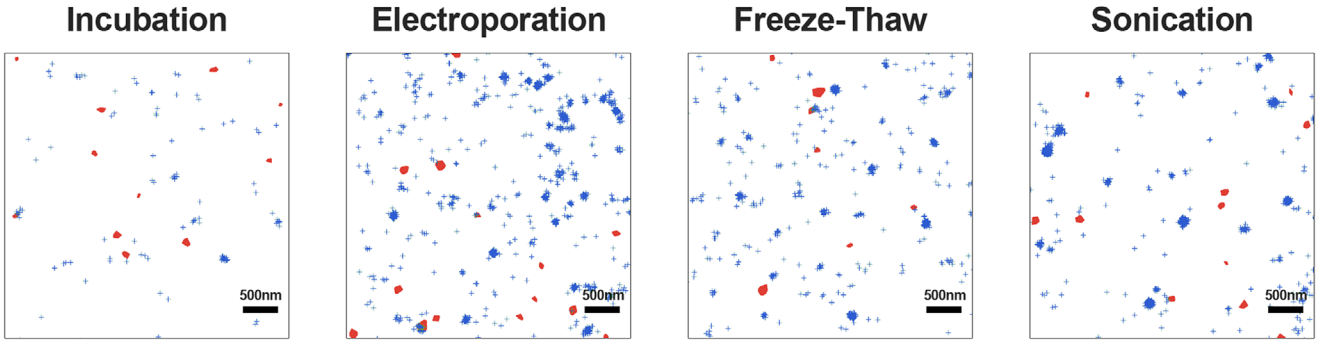

Figure 3. Representative images after DBSCAN clustering. GFP (blue crosses) can be localised within CD63+ EVs (filled red circles) after the applied loading methods.

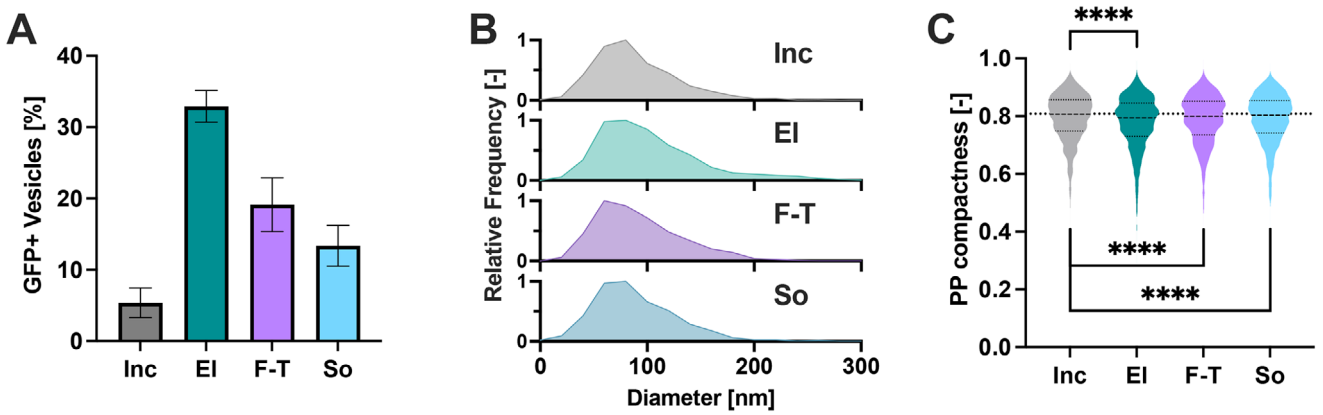

Figure 4. Characterization of loading at the single particle level by single molecule localization microscopy. A) Percent of GFP positive vesicles after applying different loading methods. Inc – Incubation, EI – Electroporation, F-T – Freeze-Thaw, So – Sonication. The data are represented as mean +/- standard deviation of three replicates (n=3) B) Size distribution of CD63+ vesicles after electroporation measured by SMLM-DBSCAN. C) The compactness of the EVs is reduced by less than 2% by all loading methods.The distributions consist of a minimum 1000 individually measured vesicles. Post hoc analysis: Ordinary one way ANOVA **** - P-value <0.0001.

EVs, which is reduced by less than 2% (Figure 4C). Moreover, the number of GFP molecules associated with an individual EV does not correlate with its compactness(Figure S10, Supporting Information). Furthermore, application of the loading procedures to GFP alone, before mixing with EVs, does not increase the colocalization (Figure S11, Supporting Information). Overall, these results indicate that the GFP cargo is not associated with EVs as GFP aggregates, which would lead to a decrease in compactness.

The single-particle analysis revealed a very broad distribution of GFP molecules in the CD63+ EV subpopulation for all loading methods (**Figure 5** Row A). For instance, after electroporation, most of the loaded EVs (22%) contained between 1 and 5 GFP, similarly to the other loading methods, while 1% of

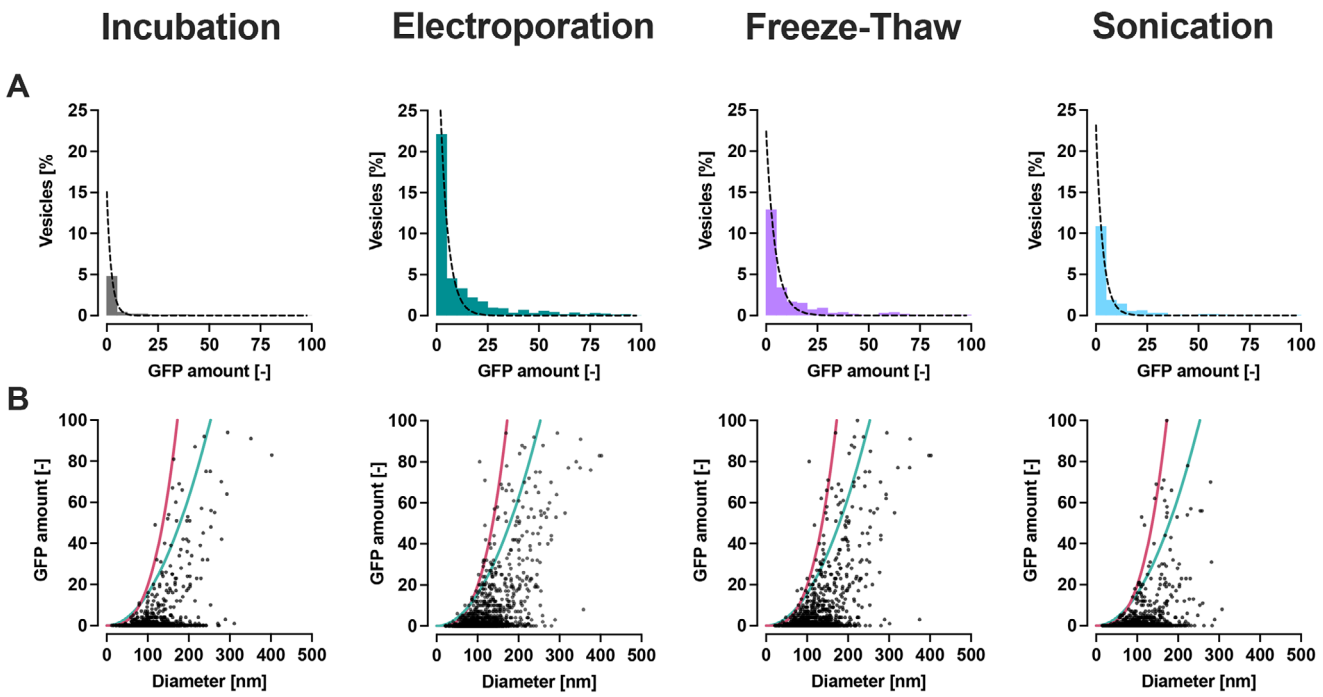

Figure 5. Characterization of distribution of cargo at the single particle level by single molecule localization microscopy. A) Distribution of the amount of GFP associated with CD63+ vesicles after the loading treatments. Vesicles that did not contain any GFP molecule were excluded for clarity. The dotted line corresponds to an exponential decay fitted to the data. B) Number of GFP molecules associated with one EV after the loading treatment as a function of EV size. The green and the red lines indicate, respectively, 10% of the maximum number of GFP molecules that could fit on the surface (S_{Max}) and 1% of the maximum number of GFP molecules that could fit in the volume (V_{Max}) of EVs. The distributions consist of a minimum 1000 individually measured vesicles.

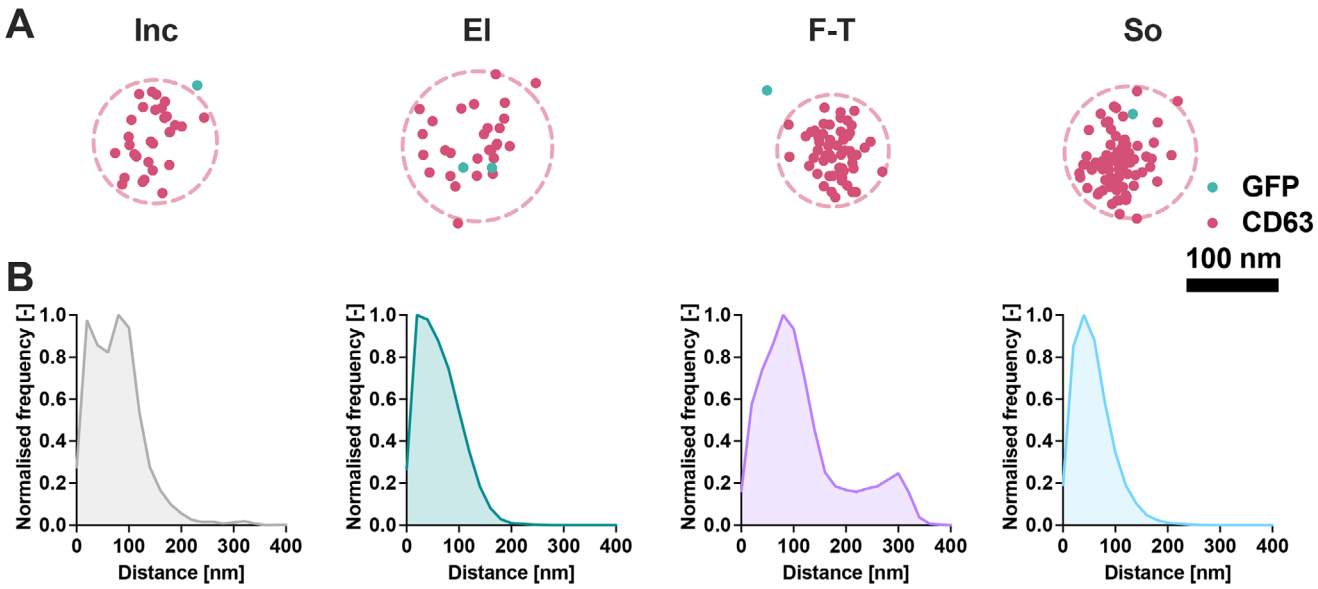

Figure 6. Distribution of GFP associated with the EVs after the loading processes. A) Representative localization data from individual EVs. The red dashed circle is an illustrative outline of the vesicles. The scale bar is 100 nm. B) Distance distribution between the nearest CD63 and GFP localizations. From left to right: Incubation, Electroporation, Freeze-Thaw, and Sonication. The distributions consist of a minimum 200000 individually measured distances between localizations.

the EVs had more than 75 GFP molecules associated (Figure 5 Row A). The shape of the probability distribution of GFPs associated with EVs could be described with a simple one phase exponential decay function. Interestingly, the same exponential function of the cargo distribution was observed when loading homogeneous liposomes (Figure S12, Supporting Information), indicating that this heterogeneity arises from the loading process.

The number of GFP molecules loaded into one single EV increases with increasing the size of the EV (Figure 5 Row B). Specifically, larger EVs in the range from 200 to 300 nm are loaded with up to 94 GFPs after electroporation. In contrast, EVs with a diameter around 100 nm rarely contain more than 20 GFP. This trend is also observed for all the investigated loading methods (Figure 5 Row B).

Assuming a hydrodynamic diameter of GFP of 4 nm, an unrealistic fully empty EV and tight packing, we estimate the theoretical limit of GFP molecules that can be loaded on the surface (S_{Max}) and in the volume (V_{Max}) of EVs. The experimentally measured number of GFP molecules loaded into EVs corresponds to either 2.5% of the theoretical amount that would fit in the volume or 4% of the amount that could be loaded on the surface area[47] (Figure 5 Row B).

We analyzed the morphology of the vesicles by looking at the distance distribution between the nearest localization signals of GFP and CD63 in dSTORM. Representative CD63 and GFP localizations in individual vesicles are shown in **Figure** 6A. The different loading methods yielded different distance distributions. The results show that after electroporation and sonication, GFP is located near CD63, therefore confirming successful loading (Figure 6B). In contrast, after freeze-thawing the distance between the nearest GFP and CD63 localizations is mostly 100 nm. The difference in the proximity distribution of the GFP and CD63 after the loading methods demonstrate a different spatial distribution of the cargo associated to the vesicles. Based on the difference in proximity distributions, freeze-thaw and incubation likely associated the cargo more on the surface, while sonication and electroporation more with the lumen.

We note that our current methodology aimed at characterizing loading heterogeneity at the individual EV level, but it does not allow to distinguish between luminal encapsulation and surface adsorption. Protease- or detergent-based assays could, in principle, provide further insight into this aspect, but they proved to be incompatible with dSTORM. For instance, protease treatment of EV interfered with EV detection by dSTORM due to degradation of surface markers required for colocalization analysis.

2.4. Conclusion

In this study we have characterized the exogenous loading of a model cargo protein into EVs at both the ensemble and single vesicle levels.

Our findings show that, in our experimental setup, electroporation emerged as the most effective loading method, achieving a percentage of loaded vesicles comparable to endogenous loading.[16] However, the overall yield was modest, with EVs associated with only a small fraction (approximately 2–4%) of their theoretical protein capacity. This suggests that exogenous EV loading may be more suitable when the delivery of smaller quantities of proteins is sufficient, for instance in the case of enzymes.

In addition to loading efficiency, we characterized the heterogeneity in the distribution of cargo molecules associated with the EV population at the single particle level using super-resolution microscopy. Importantly, across all loading methods, the distribution of cargo proteins in individual vesicles exhibited signifi-

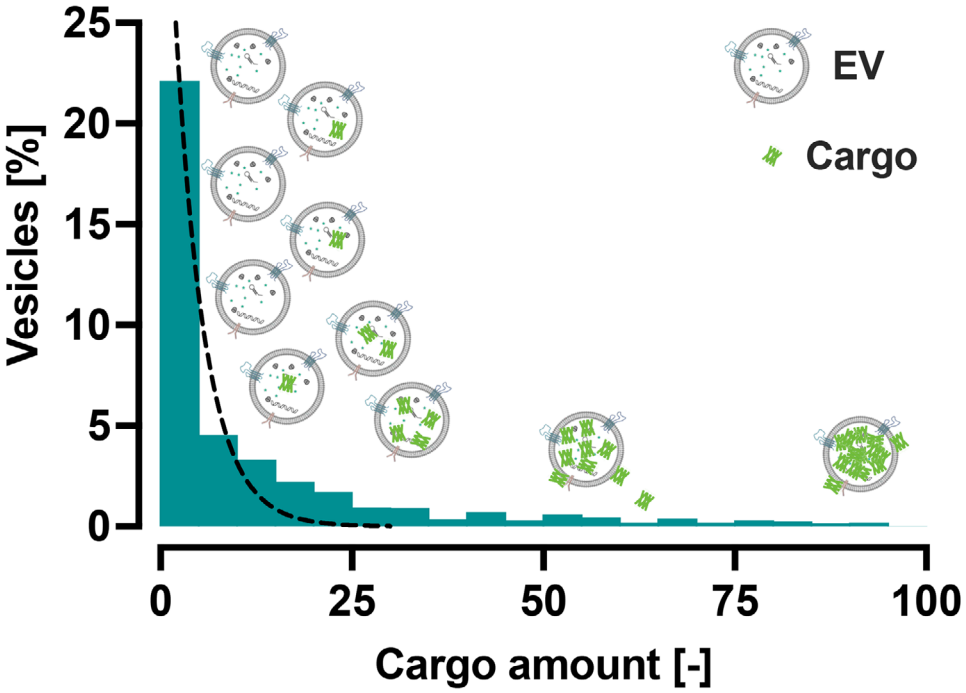

Figure 7. The distribution of cargo in the vesicle population is highly heterogeneous and follows an exponential decay pattern, with a prevalence of vesicles with no or low protein content and a minority with higher content. Vesicles that did not contain any GFP molecule were excluded for clarity. The dotted line corresponds to an exponential decay fitted to the data.

cant heterogeneity, following an exponential decay pattern. This indicated a prevalence of vesicles with lower protein content and a minority with higher content (**Figure 7**). Moreover, we observed that loading efficiency increased with EV size. The results emphasize the importance of EV processing in determining the heterogeneity of EVs.[25,26]

It is likely that a substantial portion of the proteins associated with EVs is not encapsulated within the vesicle lumen but instead adsorbed onto the surface, contributing to the formation of a protein corona. Indeed, this surface-binding phenomenon is increasingly reported in the EV field.[48–51] Depending on the application, either predominantly luminal[11,19–21,52] or surface association[12,17,53,54] can be desired.

This high heterogeneity within EVs is expected to significantly influence the biological activity of loaded EVs,[25] akin to observations made with simpler synthetic nanoparticles.[22–24,26,27] Future research should focus on functional studies to assess the effect of both loading efficiency and heterogeneity over the delivery efficiency and biological activity of engineered EVs.

3. Experimental Section

Isolation of Extracellular Vesicles (EVs): EVs were produced according to a previously published method and had been extensively characterized in previous works.[36–39] In brief, HEK293-F cells (Thermo Fisher, USA) were cultured at 37°C in chemically defined, particle- and protein-free CD293 medium (Thermo Fisher, USA) supplemented with 4mM GlutaMAX and 250 mg/L Pluronic F-68 (Thermo Fisher, USA). The culture was innoculated at $0.3*10^6$ cells/mL. The culture was stirred at 250 rpm and maintained at pH 7.1 and a dissolved oxygen concentration of 40% in a stirred tank bioreactor (DASGIP, Eppendorf) for 136 h. Conditioned media (1 L) was harvested when the cell density reached $1.8*10^7$ cells/mL with 92% viability, clarified by two centrifugation steps (the first at 200g for 10 min and the second at 3000g for 15 min), and frozen in aliquots. The 50 mL aliquots were thawed and filtered by a 0.22 μm PES syringe filter (TPP, Switzerland). To remove DNA and other nucleotide contamination, 100U of Pierce nuclease (Thermo Fisher, USA) was added to the condition media. The sample was then concentrated using an Amicon 50kDa MWCO ultrafilter (Merck Millipore, Ireland) to approximately 0.5mL. Aggregates were removed by centrifugation at 7000g for 5 min before applying size exclusion chromatography using 10mL of Sepharose CL-4B resin (Sigma-Aldrich, Germany) packed by gravity into an Econo-Pac (Bio-Rad, USA) gravity flow column. PBS was used as the elution buffer. 0.5 mL fractions were collected, and fractions 5 to 8 (corresponding to EVs) were combined together. The total protein content of EVs was quantified through Bicinchonicic Acid Assay (Thermo Fisher, USA), according to manufacturer's instruction. The particle concentration was then measured by Nanoparticle Tracking Analysis (Particle Metrix Zetaview, Germany), and particle-to-protein ratio calculated. The measured preparations showed high particle-to-protein ratios (between 2-3e+10 prt/µg of proteins), indicating highly pure EVs. Further characterization is shown in the Figures S1 and S2 (Supporting Information).

GFP Expression and Purification: The GFP plasmid for recombinant expression was codon optimized for expression in E. coli, synthesized and cloned into the pET-15b vector by Genewiz (NJ, US). E. coli BL21-GOLD (DE3) cells were used for recombinant expression. Recombinant expression was induced at OD 0.7 with 0.5 mM isopropyl D-thiogalactopyranoside (99%, PanReac AppliChem) and cells were grown for an additional 16 h at 37°C. GFP was purified by immobilized metal ion affinity chromatography (Chelating Sepharose, GE Healthcare). The protein was further purified by size exclusion chromatography using a Superdex 75 16/600 column (GE Healthcare) assembled on an ÄKTA Prime system (GE Healthcare) using PBS as eluent buffer. The final purity of the

protein was assessed by SDS-PAGE electrophoresis. Protein stocks were concentrated to above 200μM and aliquots (20μL) were frozen and stored at -20°C until use. Final concentrations were assessed by measuring absorbance at 280 nm.

Loading of sEVs: All loading experiments were performed using 10^{10} particles/mL of EV stock and 10μM GFP cargo in PBS. The loading methods followed commonly reported literature protocols: Incubation - The mixture of EVs and protein cargo was incubated at room temperature for 2 h. Electroporation - The mixture was electroporated using a NepaGene NEPA21 electroporator, using commonly reported electroporation parameters.[55–58] The poring pulse settings were 200 V for 5 ms per pulse for two pulses without polarity switching and with a decay rate of 40%. The poring pulses were followed by transfer pulses set to 20 V for 50 ms per pulse for five pulses with polarity switching and a decay rate of 10%. Sonication - The mixture was sonicated in a bath sonicator for 3 min at 37 kHz at 35°C. Freeze-Thaw - The mixture was frozen for 1 min in liquid nitrogen and thawed for 5 min in a water bath set to 50°C. The freeze-thaw cycles were repeated three times.

Size Exclusion Chromatography Coupled With Fluorescence Detection and Multi-Angle Light Scattering: After the loading procedure, the sample was centrifuged for 2 min at 10000 rcf to remove potential large micron-size aggregates that could harm the column. 40μL sample was injected at a volumetric flow rate of 0.1 $mlmin^{-1}$ into a size exclusion Tricorn-100 column of 2 ml bed volume packed with Sepharose-CL4B resin (Sigma–Aldrich, Germany) assembled on an Agilent 1200 Series HPLC system. PBS was used as eluent solution. The HPLC apparatus was connected with in-line multi-angle light scattering (MALS) detector (DAWN HELEOS II, Wyatt Technology, US) and fluorescence detector (FLD) (1260 Infinity II, Agilent Technologies, US). Rayleigh ratio data were collected by ASTRA V Software (Wyatt Technology, US). Rayleigh ratio data were despiked using a median filter, smoothed by Savitzky-Golay filtering and baseline corrected to obtain the excess Rayleigh ratios. Particle radii and the Rayleigh ratio at angle 0 (R_0) were obtained following the procedure described in ref. [39]

For the fluorescence detection, excitation and emission wavelengths for GFP were set to $\lambda_{ex} = 480$ nm and $\lambda_{em} = 520$ nm, respectively. Fluorescence gain was set to 18. The baseline was corrected by setting as reference the fluorescence value measured at 0.6 mL. The amount of loaded protein was quantified by integrating the area under the peak eluting at approximatively 1 mL via a calibration curve (Figure S3, Supporting Information).

To calculate the amount of GFP per EV particle, the amount of GFP was converted from moles to the number of molecules by multiplying with the Avogadro constant and divided with the total number of particles measured.

Bead-Based Flow Cytometry: 5 μL of exosome-human CD81 flow detection reagent (ThermoFisher, USA) (beads) was washed in 200 μL of 0.1% BSA (Sigma–Aldrich, Germany) in PBS. 10 μL of sample was diluted to 100μL and a final concentration of 0.1% BSA. The diluted sample was added to the washed beads and incubated overnight at 4°C while shaking protected from light. The beads were washed twice with 300 μL before resuspending in 100 μL FC buffer. 1.2 μL of anti-human CD81-APC (ThermoFisher, USA) conjugate was added to each sample and shaken protected from light for 1.5 h. The beads were washed twice with 200 μL before resuspension in 150 μL FC buffer and transferred to a 96 well cell culture plate (TPP, Switzerland).

The flow cytometry measurements were performed on a Beckman Coulter (USA) CytoFLEX S flow cytometer. The gain of the forward scattering was set to 199, the side scattering to 48 and the FITC fluorescence (525/40 nm bandpass filter and blue laser) to 3000. Before measuring each sample, the plate was mixed for 3 s. Measurements were recorded for 180 s. Between each sample, two water samples were injected to clear the line. Event signal heights were analyzed using a custom-made Python program. The gating thresholds for the scattering and fluorescence signals were set based on the flow cytometry events of the flow detection reagent beads. Single particle scattering events were analyzed by selecting only events with a forward scattering intensity between 65000 and 250000 and a side scattering intensity between 350000 and 175000.

dSTORM-DBSCAN: After the loading procedure, the sample was centrifuged for 2 min at 10000 rcf to remove potential large micron-size aggregates that could harm the column. 100 μL of sample containing loaded EVs was fractionated using Sepharose CL-4B resin packed into a Tricorn-10/300 column. A 400μL vesicle fraction was collected between 7.8 and 8.2 mL of the eluent. 100μL of the collected fraction was added to a freshly plasma treated 18 well μ-Slide (Ibidi, Germany). The sample was incubated for 1 h, the supernatant was aspirated and replaced with a blocking buffer (1% BSA in PBS). After 1 h, the blocking buffer was removed and 100 μL 10000x diluted anti-CD63-AlexaFluor647 (Novus Biologicals, USA) in blocking buffer was added. The sample was incubated overnight. Before imaging, the antibody solution was removed and 250 μL of a standard STORM blinking buffer was added. The sample was covered with a glass coverslip to avoid the diffusion of oxygen inside. The blinking buffer consisted of 10 mM MEA (Apollo Scientific Ltd, USA), 40 $mgmL^{-1}$ glucose (Sigma–Aldrich, Germany), 4.5% glycerin (Sigma–Aldrich, Germany), 1 μgmL^{-1} catalase (Sigma–Aldrich, germany), 50 μgmL^{-1} glucose oxidase (Sigma–Aldrich, Germany), 0.2 *mM* Tris(2-carboxyethyl)phosphine hydrochloride (Sigma–Aldrich, Germany), 1.25 *mM* KCl (Sigma–Aldrich, Germany), 1 *mM* Tris (Sigma–Aldrich, Germany) pH 7.5 and 0.5x PBS (ThermoFisher, USA). The blinking buffer was freshly prepared each time from stock solutions before imaging.

The samples were imaged using a Nikon Ti2 Eclipse inverted microscope system equipped with a ANDOR iXon DU897 (16x16μm^2 pixel size) EM-CCD camera and an SR Apochromat TIRF 100x 1.49 N.A oil immersion objective. The sample was illuminated in total internal reflection mode and the laser angle of incidence was monitored with a Photometrics Dyno CCD camera at the back focal plane of the objective. The samples were imaged sequentially with excitation at the 647 nm (125 mW at the tip) and 488 nm(80 mW at the tip) laser lines. The fluorescence emission was passed through a QUAD filter set for TIRF application (Nikon C-NSTORM QUAD 405/488/561/647). The laser power was set to 40% at a 2x magnification. 10000 images were recorded at an exposure time of 30 msec. The focus was stabilised by the Perfect Focus System (Nikon) during imaging. The image acquisition was controlled with NIS Elements Advanced (Nikon) software.

Images were analyzed by ImageJ and the ThunderSTORM plugin to detect fluorophore localization.[59] Only localizations with a precision smaller than 30 nm and a standard deviation of the point spread function (PSF) in the range from 30 to 300 nm were considered. Multi-frame emitters were combined and the locations averaged. The fluorophore localizations in both the 488 and 647 channels were combined. The datapoints were clustered by Density-Based Spatial Clustering of Applications with Noise (DBSCAN) algorithm.[60–62]

The localizations were clustered and analyzed with a custom-written Python script. The clustering parameter epsilon was set to 50 nm and the minimum number of neighbors was set to 5. For liposome sizing, the minimum number of neighbors was set to 20. The size of the vesicle was determined by constructing a convex hull around the cluster of points. At least 1600 vesicles were analyzed per sample.

Following an approach reported in the literature,[41–43,45,46] the GFP amount was quantified by measuring photophysical properties, specifically the probabilities of observing a threshold number of blinking events (Figure S13, Supporting Information). To quantify the photophysical properties of GFP, a 1 pM and 1 nM sample of GFP was prepared and imaged at the same conditions as the vesicle samples. The adjacent blinks were clustered and each cluster of blinks was considered as 1 molecule blinking. The probabilities obtained from a total of six images were combined to obtain the probability distribution of the blinks of GFP under the imaging conditions.

The GFP cargo was quantified by the measured total number of blinks taking into account the probability distribution of blinking events, which was previously characterized under the same imaging conditions (Figure S13, Supporting Information):

$$N_{tot} = \sum \rho_x N_x \quad (1)$$

where N_{tot} is the total number of blinks, ρ_x is the probability that an individual GFP molecule blinks x times, and N_x is the number of GFP molecules

that blink x times. The sum was considered up to ten blinking events, above which the probability was essentially zero.

Only CD63-positive clusters were considered as an EV and the localization composition of EVs was further analysed.[42,46,63] The GFP+ vesicle number was calculated by dividing the number of CD63+ vesicles that were also co-localized with GFP with the total number of CD63+ vesicles measured.

For the analysis of the morphology of the vesicles, a convex hull was constructed around the vesicle cluster localizations and the Polsby-Popper test was applied.[44] The compactness index compares the area of the vesicle to its perimeter:

$$PPcompactness = \frac{4\pi A}{P^2} \quad (2)$$

where A is the area of the vesicle and P its perimeter. A perfectly circular vesicle would have a PP compactness of 1.

Liposome Preparation: Liposomes were prepared by the lipid film hydration method. In brief, 0.75mg of Cholesterol (Sigma–Aldrich, Germany) 0.5025 mg of Sphingomyelin (Sigma–Aldrich, Germany), 1.245 mg OPPC (Sigma–Aldrich, Germany) and 0.0125mg of DiO or DiD (Sigma–Aldrich, Germany) were disolved in 2mL of chloroform from stock solutions in a round bottom flask. The chloroform was evaporated under a stream of nitrogen at room temperature. The remaining chloroform was removed by rotoevaporation at room temperature and 250 mbar pressure for 12 h. The lipid film was hydrated while gently mixing in 10mL of PBS until the entire lipid film detached. The solution was then freeze-thawed three times and extruded through a filter (Cytiva, USA). Different filters with nominal pore sizes of 50, 100, 200, and 400nm were used to prepare the different sized liposomes.

NTA: Measurements were performed on a Zetaview NTA (Particle Metrix, Germany). Before each series of measurements, the system was calibrated using polystyrene beads following the manufacturer's instructions. Samples were diluted in PBS (Thermo Fisher) (typically 1000-fold) to achieve low concentrations suitable for NTA measurements. The sensitivity was set to 85 and the shutter to 125. For each sample, 11 positions were considered for analysis.

Supporting Information

Supporting Information is available from the Wiley Online Library or from the author.

Acknowledgements

The authors thank the ScopeM center at ETH Zürich for providing technical support. The authors also thank the BOW Project for funding (FET Proactive programme under grant agreement No 952183).

Conflict of Interest

The authors declare no conflict of interest.

Data Availability Statement

The data that support the findings of this study are available from the corresponding author upon reasonable request.

Keywords

cargo loading, cargo quantification, extracellular vesicles, exogeneous engineering, heterogeneity

Received: March 21, 2025
Revised: June 6, 2025
Published online: September 17, 2025

[1] R. Kalluri, V. S. LeBleu, *Science* **2020**, *367*, 6478.
[2] J. A. Welsh, D. C. Goberdhan, L. O'Driscoll, E. I. Buzas, C. Blenkiron, B. Bussolati, H. Cai, D. Di Vizio, T. A. Driedonks, U. Erdbrügger, J. M. Falcon-Perez, Q.-L. Fu, A. F. Hill, M. Lenassi, S. K. Lim, M. G. Mahoney, S. Mohanty, A. Möller, R. Nieuwland, T. Ochiya, S. Sahoo, A. C. Torrecilhas, L. Zheng, A. Zijlstra, S. Abuelreich, R. Bagabas, P. Bergese, E. M. Bridges, M. Brucale, D. Burger, et al., *J. Extracell. Vesicles* **2024**, *13*, e12404.
[3] M. Tkach, C. Théry, *Cell* **2016**, *164*, 1226.
[4] L. A. Mulcahy, R. C. Pink, D. R. F. Carter, *J. Extracell. Vesicles* **2014**, *3*, 24641.
[5] M. Yáñez-Mó, P. R. Siljander, Z. Andreu, A. B. Zavec, F. E. Borràs, E. I. Buzas, K. Buzas, E. Casal, F. Cappello, J. Carvalho, E. Colás, A. Cordeiro-Da Silva, S. Fais, J. M. Falcon-Perez, I. M. Ghobrial, B. Giebel, M. Gimona, M. Graner, I. Gursel, M. Gursel, N. H. Heegaard, A. Hendrix, P. Kierulf, K. Kokubun, M. Kosanovic, V. Kralj-Iglic, E. M. Krämer-Albers, S. Laitinen, C. Lässer, T. Lener, et al., *J. Extracell. Vesicles* **2015**, *4*, 1.
[6] G. Van Niel, G. D'Angelo, G. Raposo, *Nat. Rev. Mol. Cell Biol.* **2018**, *19*, 213.
[7] L. Margolis, Y. Sadovsky, *PLoS Biol.* **2019**, *17*, e3000363.
[8] I. K. Herrmann, M. J. A. Wood, G. Fuhrmann, *Nat. Nanotechnol.* **2021**, *16*, 748.
[9] G. Fuhrmann, A. Serio, M. Mazo, R. Nair, M. M. Stevens, *J. Controlled Release* **2015**, *205*, 35.
[10] M. S. Kim, M. J. Haney, Y. Zhao, V. Mahajan, I. Deygen, N. L. Klyachko, E. Inskoe, A. Piroyan, M. Sokolsky, O. Okolie, S. D. Hingtgen, A. V. Kabanov, E. V. Batrakova, *Nanomed.: Nanotechnol., Biol., Med.* **2016**, *12*, 655.
[11] M. J. Haney, N. L. Klyachko, Y. Zhao, R. Gupta, E. G. Plotnikova, Z. He, T. Patel, A. Piroyan, M. Sokolsky, A. V. Kabanov, E. V. Batrakova, *J. Controlled Release* **2015**, *207*, 18.
[12] L. Alvarez-Erviti, Y. Seow, H. Yin, C. Betts, S. Lakhal, M. J. Wood, *Nat. Biotechnol.* **2011**, *29*, 341.
[13] S. A. Kooijmans, S. Stremersch, K. Braeckmans, S. C. D. Smedt, A. Hendrix, M. J. Wood, R. M. Schiffelers, K. Raemdonck, P. Vader, *J. Controlled Release* **2013**, *172*, 229.
[14] T. N. Lamichhane, R. S. Raiker, S. M. Jay, *Mol. Pharmaceutics* **2015**, *12*, 3650.
[15] M. Piffoux, J. Volatron, K. Cherukula, K. Aubertin, C. Wilhelm, A. K. Silva, F. Gazeau, *Adv. Drug Delivery Rev.* **2021**, *178*, 113972.
[16] A. M. Silva, E. Lázaro-Ibáñez, A. Gunnarsson, A. Dhande, G. Daaboul, B. Peacock, X. Osteikoetxea, N. Salmond, K. P. Friis, O. Shatnyeva, N. Dekker, *J. Extracell. Vesicles* **2021**, *10*, e12130.
[17] G. Corso, W. Heusermann, D. Trojer, A. Görgens, E. Steib, J. Voshol, A. Graff, C. Genoud, Y. Lee, J. Hean, J. Z. Nordin, O. P. Wiklander, S. El Andaloussi, N. Meisner-Kober, *J. Extracell. Vesicles* **2019**, *8*, 1.
[18] J. Cardellini, K. Normak, M. Gerlt, K. Makasewicz, C. Seiffert, U. Capasso Palmiero, S. Ye, M. A. González Gómez, Y. Piñero, J. Rivas, A. Bongiovanni, P. Bergese, P. Arosio, *Adv. Healthcare Mater.* **2025**, *14*, 2403264.
[19] C. Chen, M. Sun, J. Wang, L. Su, J. Lin, X. Yan, *J. Extracell. Vesicles* **2021**, *10*, e12163.
[20] C. Chen, Y. Li, Q. Wang, N. Cai, L. Wu, X. Yan, *Anal. Bioanal. Chem.* **2023**, *415*, 1287.
[21] N. M. Lowe, R. R. Mizenko, B. B. Nguyen, K. L. Chiu, V. Arun, A. Panitch, R. P. Carney, *J. Extracellular Biol.* **2024**, *3*, e70003.

[22] C. Saunders, J. E. J. Foote, J. P. Wojciechowski, A. Cammack, S. V. Pedersen, J. J. Doutch, H. M. G. Barriga, M. N. Holme, J. Penders, M. Chami, A. Najer, M. M. Stevens, *ACS Nano* **2023**, *17*, 11713.
[23] T. Sych, J. Schlegel, H. M. G. Barriga, M. Ojansivu, L. Hanke, F. Weber, R. Beklem Bostancioglu, K. Ezzat, H. Stangl, B. Plochberger, J. Laurencikiene, S. El Andaloussi, D. Fürth, M. M. Stevens, E. Sezgin, *Nat. Biotechnol.* **2024**, *42*, 587.
[24] J.-M. Rabanel, V. Adibnia, S. F. Tehrani, S. Sanche, P. Hildgen, X. Banquy, C. Ramassamy, *Nanoscale* **2019**, *11*, 383.
[25] M. Manno, A. Bongiovanni, L. Margolis, P. Bergese, P. Arosio, *Nat. Rev. Bioeng.* **2024**, *3*, 68.
[26] S. M. Stavis, J. A. Fagan, M. Stopa, J. A. Liddle, *ACS Appl. Nano Mater.* **2018**, *1*, 4358.
[27] J. Morla-Folch, A. Ranzenigo, Z. A. Fayad, A. J. P. Teunissen, *Small* **2024**, *20*, 2307502.
[28] C. Saunders, C. A. De Villiers, M. M. Stevens, *AAPS J.* **2023**, *25*, 94.
[29] S. I. van de Wakker, J. Bauzá-Martinez, C. Ríos Arceo, H. Manjikian, C. J. B. Snijders Blok, M. T. Roefs, E. Willms, R. G. C. Maas, M. F. Pronker, O. G. de Jong, W. Wu, A. Görgens, S. El Andaloussi, J. P. G. Sluijter, P. Vader, *J. Extracell. Vesicles* **2024**, *13*, 12396.
[30] A. Musicò, A. Zendrini, S. G. Reyes, V. Mangolini, L. Paolini, M. Romano, A. Papait, A. R. Silini, P. Di Gianvincenzo, A. Neva, M. Cretich, O. Parolini, C. Almici, S. E. Moya, A. Radeghieri, P. Bergese, *Nanoscale Horiz.* **2025**, *10*, 104.
[31] E. Willms, H. J. Johansson, I. Mäger, Y. Lee, K. E. M. Blomberg, M. Sadik, A. Alaarg, C. E. Smith, J. Lehtiö, S. El Andaloussi, M. J. A. Wood, P. Vader, *Sci. Rep.* **2016**, *6*, 22519.
[32] O. P. Wiklander, J. Z. Nordin, A. O'Loughlin, Y. Gustafsson, G. Corso, I. Mäger, P. Vader, Y. Lee, H. Sork, Y. Seow, N. Heldring, L. Alvarez-Erviti, C. I. E. Smith, K. Le Blanc, P. Macchiarini, P. Jungebluth, M. J. A. Wood, S. El Andaloussi, *J. Extracell. Vesicles* **2015**, *4*, 26316.
[33] B. Z. Wang, L. J. Luo, G. Vunjak-Novakovic, *Adv. Healthcare Mater.* **2022**, *11*, 2101557.
[34] I. Nakase, K. Noguchi, A. Aoki, T. Takatani-Nakase, I. Fujii, S. Futaki, *Sci. Rep.* **2017**, *7*, 1.
[35] J. Zhuang, J. Tan, C. Wu, J. Zhang, T. Liu, C. Fan, J. Li, Y. Zhang, *Nucleic Acids Res.* **2020**, *48*, 8870.
[36] C. Paganini, B. Hettich, M. R. Kopp, A. Eördögh, U. Capasso Palmiero, G. Adamo, N. Touzet, M. Manno, A. Bongiovanni, P. Rivera-Fuentes, J.-C. Leroux, P. Arosio, *Adv. Healthcare Mater.* **2022**, *11*, 2100021.
[37] C. Paganini, H. Boyce, G. Libort, P. Arosio, *Adv. Healthcare Mater.* **2023**, *12*, 2202232.
[38] C. Paganini, U. Capasso Palmiero, S. Picciotto, A. Molinelli, I. Porello, G. Adamo, M. Manno, A. Bongiovanni, P. Arosio, *Small* **2023**, *19*, 2204736.
[39] K. Normak, M. Papp, M. Ullmann, C. Paganini, M. Manno, A. Bongiovanni, P. Bergese, P. Arosio, *Anal. Chem.* **2023**, *95*, 12443.
[40] R. P. McNamara, Y. Zhou, A. B. Eason, J. T. Landis, M. G. Chambers, S. Willcox, T. A. Peterson, B. Schouest, N. J. Maness, A. G. MacLean, L. M. Costantini, J. D. Griffith, D. P. Dittmer, *J. Extracell. Vesicles* **2022**, *11*, 3.
[41] A. Saftics, S. Abuelreich, E. Romano, I. Ghaeli, N. Jiang, M. Spanos, K. M. Lennon, G. Singh, S. Das, K. Van Keuren-Jensen, T. Jovanovic-Talisman, *J. Extracell. Vesicles* **2023**, *12*, 12346.
[42] F. Fricke, J. Beaudouin, R. Eils, M. Heilemann, *Sci. Rep.* **2015**, *5*, 14072.
[43] T. N. Baldering, M. S. Dietz, K. Gatterdam, C. Karathanasis, R. Wieneke, R. Tampé, M. Heilemann, *Mol. Biol. Cell* **2019**, *30*, 1369.
[44] D. D. Polsby, R. Popper, *SSRN Electron. J.* **1991**, *9*, 301.
[45] S.-H. Lee, J. Y. Shin, A. Lee, C. Bustamante, *Proc. Natl. Acad. Sci. USA* **2012**, *109*, 17436.
[46] G. Hummer, F. Fricke, M. Heilemann, *Mol. Biol. Cell* **2016**, *27*, 3637.
[47] A. Zendrini, G. Guerra, K. Sagini, T. Vagner, D. Di Vizio, P. Bergese, *Colloids Surf., B* **2022**, *218*, 112728.
[48] E. I. Buzas, *Nat. Cell Biol.* **2022**, *24*, 1322.
[49] M. Wolf, R. W. Poupardin, P. Ebner-Peking, A. C. Andrade, C. Blöchl, A. Obermayer, F. G. Gomes, B. Vari, N. Maeding, E. Eminger, H. Binder, A. M. Raninger, S. Hochmann, G. Brachtl, A. Spittler, T. Heuser, R. Ofir, C. G. Huber, Z. Aberman, K. Schallmoser, H. Volk, D. Strunk, *J. Extracell. Vesicles* **2022**, *11*, e12207.
[50] E. Tóth, L. Turiák, T. Visnovitz, C. Cserép, A. Mázló, B. W. Sódar, A. I. Försönits, G. Petővári, A. Sebestyén, Z. Komlósi, L. Drahos, g. Kittel, G. Nagy, A. Bácsi, d. Dénes, Y. S. Gho, K. Szabó-Taylor, E. I. Buzás, *J. Extracell. Vesicles* **2021**, *10*, 11.
[51] A. Musicò, R. Zenatelli, M. Romano, A. Zendrini, S. Alacqua, S. Tassoni, L. Paolini, C. Urbinati, M. Rusnati, P. Bergese, G. Pomarico, A. Radeghieri, *Nanoscale Adv.* **2023**, *5*, 4703.
[52] Y. Oka, K. Tanaka, Y. Kawasaki, *Sci. Rep.* **2023**, *13*, 17436.
[53] J. A. Peruzzi, T. F. Gunnels, H. I. Edelstein, P. Lu, D. Baker, J. N. Leonard, N. P. Kamat, *Nat. Commun.* **2024**, *15*, 5618.
[54] K. Dooley, R. E. McConnell, K. Xu, N. D. Lewis, S. Haupt, M. R. Youniss, S. Martin, C. L. Sia, C. McCoy, R. J. Moniz, O. Burenkova, J. Sanchez-Salazar, S. C. Jang, B. Choi, R. A. Harrison, D. Houde, D. Burzyn, C. Leng, K. Kirwin, N. L. Ross, J. D. Finn, L. Gaidukov, K. D. Economides, S. Estes, J. E. Thornton, J. D. Kulman, S. Sathyanarayanan, D. E. Williams, *Mol. Ther.* **2021**, *29*, 1729.
[55] S. Inano, T. Kitano, *Plos one* **2024**, *19*, e0310083.
[56] T. Takenaka, S. Nakai, M. Katayama, M. Hirano, N. Ueno, K. Noguchi, T. Takatani-Nakase, I. Fujii, S. S. Kobayashi, I. Nakase, *Int. J. Pharm.* **2019**, *572*, 118762.
[57] K. Noguchi, M. Hirano, T. Hashimoto, E. Yuba, T. Takatani-Nakase, I. Nakase, *Anticancer Res.* **2019**, *39*, 6701.
[58] A. J. Lennaárd, D. R. Mamand, R. J. Wiklander, S. El Andaloussi, O. P. Wiklander, *Pharmaceutics* **2021**, *14*, 38.
[59] M. Ovesný, P. Křížek, J. Borkovec, Z. Švindrych, G. M. Hagen, *Bioinformatics* **2014**, *30*, 2389.
[60] M. Ester, H.-P. Kriegel, J. Sander, X. Xu, in *Proceedings of the Second International Conference on Knowledge Discovery and Data Mining*, KDD'96. AAAI Press, Washington DC **1996**, p. 226.
[61] E. Schubert, J. Sander, M. Ester, H. P. Kriegel, X. Xu, *ACM Trans. Database Syst.* **2017**, *42*, 1.
[62] I. M. Khater, I. R. Nabi, G. Hamarneh, *Patterns* **2020**, *1*, 100038.
[63] N. Durisic, L. L. Cuervo, M. Lakadamyali, *Curr. Opin. Chem. Biol.* **2014**, *20*, 22.